Six dimensional propagation of the H_2 molecule confined in a Single-Walled Carbon Nanotube

Manel Mondelo-Martell, Fermín Huarte-Larrañaga*

Universitat de Barcelona
Departament de Química Física & Institut de Química Teòrica i Computacional.

Abstract

A study on the quantum dynamics of the hydrogen molecule embedded in the hollow cavity of a single-walled carbon nanotube is presented, taking into account for the first time all six degrees of freedom of the confined molecule. A set of initial eigenstates of the trapped H_2 molecule are propagated for 500 fs using the State Average Multiconfigurational Time-dependent Hartree approach. An initial linear momentum is added to the hydrogen molecule in order to mimic high temperature behavior, forming an angle of 0° and 45° with respect to the nanotube's axis; an additional propagation is carried out without adding any extra momentum. The wave packet dynamics are analyzed using projections and overlap functions in the appropriate degrees of freedom. The study reveals little correlation between the translation of the confined molecule along the nanotube and the remaining degrees of freedom.

Keywords: Hydrogen, carbon Nanotubes, Storage devices, Quantum dynamics, Confinement Effects

*Cooresponding author.
email: fermin.huarte@ub.edu

1. Introduction

In the last few years the development of new storage devices for low-density gaseous species has become a field of intensive research. Their interest arises with two basic objectives in mind: to store large amounts of potential fuels in order to make their transport from the production centers feasible, and to capture known pollutants from the atmosphere to prevent, for instance, the greenhouse effect[1]. A paradigmatic case of potential fuel for the near future, due to its high efficiency and low impact in the environment, is hydrogen. Nanostructured materials, such as Carbon Nanotubes (CNT) or some Metal-organic Frameworks (MOFs) show the potential to be used for this purpose[1, 2, 3, 4]. A paradigmatic case is the research on hydrogen storage in nanostructured materials, such as Carbon Nanotubes (CNTs) or Metal-organic Frameworks (MOFs) [3, 5, 6, 7, 8, 9, 10, 11], given the potentiality of this gas a fuel for the near future. Due to its large economical interest, the storage of hydrogen in nanostructured materials has been largely studied both theoretically and experimentally, specially in the last few years. The research carried out in this kind of systems has shown the effectiveness of some of these materials as storage devices. A collateral effect of gas adsorption in nanostructures is the distortion of the confined molecules at the molecular level when the cavities in which they are trapped are of the order of the nanometer. These distortions, which are changes of the electronic structure and the dynamics of confined species, were first studied by Beenakker[12] *et al* in the middle 90s. In the early 2000s relevant studies of the hydrogen molecule in confining environments, including a quantum treatment of the nuclei, were carried out by Yildirim *et al* [7, 13, 14] in different

carbon structures. Gray and co–workers latter calculated the distortions in the rotation and translation of hydrogen in narrow carbon nanotubes using a four–dimensional model [15]. Lately, more complex studies have appeared on similar systems: the first 5–D quantum study of hydrogen in a carbon nanotube was carried out by one of us [16], and Bazic and co–workers have studied H_2 confined in different nanostructures such as metal–organic frameworks (MOFs) and endofullerenes. More recently, we carried out a rigorous analysis of the hydrogen molecule confined in different carbon nanotubes correlating the eigenstates of the trapped molecule with those of the free molecule [17]. The importance of these studies lies in the fact that they would not only allow a better understanding of the affinity of the confined molecules by the adsorbent, but they may also allow the discovery of new potential applications for nanostructured materials. A particularly interesting example of these novel applications are quantum sieves, which allow the separation of isotopomers of a given molecule, like H_2 and D_2, due to the different Zero-point energy (ZPE) of molecules with different mass [18, 19, 20, 4]. Also, some investigations point to the possibility of controlling chemical reactions at the molecular level using nanostructured materials[21].

Our aim in this work has been to go one step further with respect to previous simulations and carry out full dimensional (6D) propagations for a single hydrogen molecule confined in an (8,0) Single walled carbon nanotube. Unlike Refs [7, 15, 16, 17], the hydrogen molecule is here able to diffuse along the CNT axis. This is done in a fully quantum mechanical approach in order to gain insight of the quantum confinement effects at an intimate level. In spite of the number of studies in this kind of confined systems, to

our knowledge few have been made which take into account the diffusion of a molecule along a nanotube [22], and this is the first one to take into account all possible degrees of freedom of the adsorbate. In order to see the coupling between the degrees of freedom when a hydrogen molecule is diffusing along the nanotube we employ the following strategy. First, a set of functions is obtained simulating the eigenstates of a trapped H_2 molecule. These eigenstates are then given a linear impulse along the nanotube axis with different impingement angles and propagated in time. The outcome of these propagations is analyzed using several tools based on wave functions projections and overlap functions to see whether the nature of the eigenstates is conserved when the confined wave packet travels along the nanotube axis.

The work is therefore structured as follows. In Section 2 the model used to describe the system is presented. Then the relevant features of the computational tools are outlined in Section 3, focusing first on the Multiconfigurational Time-dependent Hartree approach. The remainder of Section 3 describes the procedure followed in the dynamics simulation: the preparation of the set of initial states, the simultaneous propagation and the description of the tools used to analyze them. The results of the study are discussed in Section 4 and our conclusions summarized in Section 5.

2. Description of the model

Our system of study (hereafter, H_2@SWNT) consists on a single hydrogen molecule confined in the hollow cavity of a (8,0) Single-walled Carbon Nanotube. We implemented a 6–dimensional (6D) Hamiltonian within the rigid nanotube approximation, that is, we take into account explicitly all de-

grees of freedom (DOFs) of the hydrogen molecule, but neglect the vibration of the carbon atoms. To obtain the structure of the nanotube, a geometrical optimization of its unit cell was carried out using a B3LYP functional and a 6-21G basis set with the Crystal09 software[23, 24] . The full nanotube is then represented by the concatenation of 20 unit cells, each one with a length of 8 bohr, in order to mimic an infinitely large structure and therefore minimize any edge effects.

Regarding the hydrogen molecule, the six DOFs are chosen as the internuclear H–H distance (ρ), the polar angle of the diatomic vector with respect to the nanotube's axis (θ), the azimuthal angle (ϕ), and the Cartesian coordinates of the c.o.m. of the diatom (x,y and z, being z collinear with the nanotube's axis) (Figure 1). The 6D Hamiltonian reads:

$$\hat{H}_{6D} = -\frac{\hbar^2}{2\mu_{H_2}}\left(\frac{\partial^2}{\partial\rho^2} + \frac{2}{\rho}\frac{\partial}{\partial\rho} + \frac{1}{\rho^2}\frac{\partial^2}{\partial\theta^2} + \frac{1}{\rho^2}\frac{1}{\sin^2\theta}\frac{\partial^2}{\partial\phi^2}\right) - \frac{\hbar^2}{2m_{H_2}}\left(\frac{\partial^2}{\partial x^2} + \frac{\partial^2}{\partial y^2} + \frac{\partial^2}{\partial z^2}\right) + \hat{V}(\rho,\theta,\phi,x,y,z), \quad (1)$$

with μ_{H_2} and m_{H_2} being respectively the reduced mass and the total mass of the hydrogen molecule. Hence, all degrees of freedom are explicitly defined and all couplings allowed.

The potential energy term is a 6 dimensional function of the coordinates of the hydrogen molecule. Since the Van der Waals interactions are the ones ruling the behavior of the system, we represent the potential energy surface (PES) as a sum of Lennard–Jones pair potentials — as done in previous studies on similar systems [15, 16, 17]—. Additionally, the covalent interaction between the hydrogen atoms is represented by a Morse potential [25]. The

PES then has the form:

$$\hat{V}_{6D} = V_{H-H}(\rho) + V_{C-H}(\rho, \theta, \phi, x, y, z), \tag{2}$$

$$\hat{V}_{C-H}(\rho, \theta, \phi, x, y, z) = \sum_{i=1}^{2} \sum_{j=1}^{Nc} V_{i,j}^{LJ}(d_{H_i - C_j}), \tag{3}$$

with parameters $D_e = 0.1746$ hartree, $a = 1.0271$ bohr^{-1} and $R_e = 1.4$ bohrs for the Morse potential, and $\epsilon = 2.82$ Å and $\sigma = 0.0605$ kcal/mol for the Lennard–Jones interaction. See Ref. [17] for a discussion about the suitability of these parameters.

3. Simulation details

3.1. Wave function representation

The propagations have been carried out using the Multiconfigurational Time-dependent Hartree (MCTDH) approach[26, 27] . This method allows an efficient propagation of multidimensional wave packets due to the use of a two-layer representation for the wave functions: a relatively small basis set of time-dependent, low-dimensional basis functions, known as Single-Particle Functions (SPFs, $\varphi_{j_k}^{(k)}(Q_k, t)$), which in turn are expanded in a time-independent basis of primitive functions. The *Ansatz* is then constructed as a sum of configurations, each one being a Hartree product of SPFs:

$$\Psi(Q_1, \ldots, Q_p, t) = \sum_{j_1=1}^{n_1} \cdots \sum_{j_p=1}^{n_p} A_{j_1 \cdots j_p}(t) \prod_{k=1}^{p} \varphi_{j_k}^{(k)}(Q_k, t). \tag{4}$$

And the representation of the SPFs on the primitive basis of time-independent functions reads:

$$\varphi_j^{(k)}(Q_k) = \sum_{l=1}^{N_k} a_{l_j}^{(k)} \chi_l^{(k)}(Q_k), \tag{5}$$

where the χ functions are usually a Discrete Variable Representation (DVR) or Fast Fourier Transform (FFT) grid. Equation 4, in combination with the Dirac-Frenkel variational principle, yields a system of coupled equations of motion for the system which must be integrated to solve the dynamics of the problem. This two-layer approach allows an important decrease of the size of the matrices during the integration of the equations of motion.

Another conceptual advantage of the MCTDH approach is that, since the wave function is represented as a sum of configurations, the correlation between the degrees of freedom is readily seen by the coefficients of the linear combination: for a separable system without correlation between the degrees of freedom, a single Hartree product would be enough to describe the whole system. This tool can therefore be used to analyze qualitatively the coupling between the degrees of freedom.

In the present work we have used a particular variant of the MCTDH approach: the State Averaged MCTDH method (SA-MCTDH) developed by Manthe [28]. This scheme allows the simultaneous propagation of several independent wave packets under a orthogonality constraint in a way that, in general, this simultaneous propagation is more efficient than the propagation of the individual wave packets. This method is particularly useful to obtain nuclear eigenstates of a given system by successive application of the Boltzmann operator [28, 29]. In our calculations we have taken advantage of both particularities: the Boltzmann operator has been used to obtain a set of physically meaningful states, and these states are next propagated simultaneously –this simultaneous propagation being more efficient than the individual propagation of multiple wave packets–.

In our model, each degree of freedom is represented by a set of 1D SPFs. The primitive basis sets, listed in Table 1, are chosen as a FFT equidistant grid for the ρ, ϕ, x, y and z DOFs. For the remaining degree of freedom (θ) the cot–DVR [30] is used in order to avoid a singularity in the $\frac{1}{\sin\theta}$ term of the Hamiltonian (see Equation 1).

Regarding the SPF basis two comments ought to be made. First, comparing the size of the primitive and SPF basis, the computational saving introduced by MCTDH with respect to standard wave packet approaches is evident. Secondly, the degrees of freedom with more correlation require a higher SPFs basis in order to take all this effects into account. Thus, from our converged MCTDH basis it can be predicted that the most correlated DOFs are the x, y translations and the rotational coordinates while vibration remains essentially uncoupled in our simulations.

Finally, a quartic complex absorbing potential (CAP) with length 4 Å has been added in the z coordinate in order to prevent any aliasing of the wave packet when it reaches the edge of the simulation grid.

3.2. Initial state calculation

Since solving the Time-dependent Schrödinger equation is an initial value problem, it is important to obtain physically meaningful initial states in order to extract correct information from a propagation. This initial state could be constructed, following the approach in Ref [22], as a direct product of the eigenstates of a free hydrogen molecule for the internal coordinates (ρ, θ and ϕ) and Gaussian functions for the c.o.m coordinates (x, y and z). However, as shown in a previous study[17], there are important deviations from this separable model when the hydrogen molecule is confined in a (8,0) CNT.

Table 1: Numerical details of the MCTDH wave function basis set: n_i labels the SPF basis set size, N_i the primitive basis set size, (q_{min}, q_{max}) correspond to the representation grid edges and $< q_i >_0$ the initial position expectation value. Magnitudes are given in bohr or radians, correspondingly.

q_i	n_i	q_{min}	q_{max}	N_i	$\langle q_i \rangle_0$
ρ	2	0.5	5.0	32	1.41
θ	5	0.0	π	64	$\pi/2$
ϕ	6	0.0	2π	64	0.0
x	4	-3.5	3.5	32	0.0
y	4	-3.5	3.5	32	0.0
z	5	-18.0	18.0	128	-1.36

Therefore, in order to obtain more realistic initial states for the propagation, the initial states were calculated directly as eigenstates of the H_2 confined molecule. Given that the potential is essentially unbound along z, a virtual harmonic potential was added in this degree of freedom, centered in the center of a unit cell, where the potential energy is a minimum (Fig 2). This potential allows us to artificially *trap* the gas molecule and obtain eigenstates, with only small dispersion along the z dimension but taking into account all possible distortions due to the effect of the confining potential and the coupling between the degrees of freedom. Based on the results of the 5D calculations on the same system found in Refs [16, 17], the force constant for the virtual *trapping* potential was chosen to be 200 cm^{-1}, in a way that there were no excitations in the z coordinate for the first 10 excited states of the trapped system. The details on the SPF basis set used to compute these eigenstates is shown in the first column of Table 2. Note that due to the large

Table 2: Basis set size (n_i) in the different degrees of freedom (q_i) for the three calculations in the present work: initial state calculation with trapping potential, and propagation of a set of wave packets with $\alpha = 0°$ and $\alpha = 45°$ initial conditions.

	Iterative Diagonalization	Collinear propagation	$\alpha = 45°$ propagation
$\boldsymbol{q_i}$	$\boldsymbol{n_i}$	$\boldsymbol{n_i}$	$\boldsymbol{n_i}$
ρ	2	2	2
θ	4	5	5
ϕ	6	6	6
x	4	4	5
y	4	4	5
z	1	5	5

force constant used in the trapping potential, a single SPF can be used in the z coordinate. Employing this basis set, the SA-MCTDH scheme was applied to diagonalize the Boltzmann operator at a reference temperature of 300 K. After 20 iterations the energies of a total of 11 states were converged. These are all eigenstates significantly populated at 298 K according to a Boltzmann thermal distribution.

3.3. Propagation of the initial states

The states obtained as reported above have a very low initial linear momentum in the z coordinate and are therefore not well suited for time propagation. In order to simulate the diffusion of the hydrogen molecule inside the nanotube, the linear momentum distribution of H_2's c.o.m in the z coordinate was shifted to match a mean value of 25.6 meV, with an indetermination of

9.39 meV. This energy value corresponding to the most probable kinetic energy of a particle with mass m_{H_2} following a Maxwell–Boltzmann distribution at a temperature of 298 K.

Two sets of propagations were run with different impinging angles α between the linear momentum vector and the nanotube axis: 0° and 45°. For each set, the propagation of the set of initial wave packets was carried out simultaneously during a total of 500 fs. For angles α significantly larger than 45°, the repulsion coming from the nanotube walls proved to be too large for a satisfactory convergence of the calculation, and therefore no propagations were carried out beyond this limiting value.

Although one may naively employ the same MCTDH basis employed in the eigenstate calculation, we expect distortions of the wave functions as it evolves along the nanotube axis. This will basically the case in the z coordinate where the potential energy landscape changes drastically but also in the x and y DOFs for the $\alpha = 45°$ case. For this reason the SPFs basis set used to generate the initial states was expanded in order to provide a flexible enough basis and allow for the convergence of the calculations. See in Table 2 the MCTDH basis set representation in the $\alpha = 0°$ (second column) and $\alpha = 45°$ (third column).

3.4. Analysis of the wave packets

The dynamics propagation of the H_2@CNT eigenstates is studied following two different and complementary approaches. Since the direct observation of the full wave function evolution is not possible due to the high dimensionality of the wave packets, the first tool at our disposal is the projection onto relevant subspaces. This projection allows us to reduce the

dimensionality of the functions, yielding a result which can be plotted and visualized:

$$\mid \Psi \mid^2 (\vec{r}, t) = \langle \Psi(\vec{R}; \vec{r}, t) \mid \Psi(\vec{R}; \vec{r}, t) \rangle, \tag{6}$$

where $\vec{R}$ and $\vec{r}$ represent the integrated and the projection subspaces, respectively.

Through this method we are able to extract relevant information about particular degrees of freedom of the system, but on the other hand it may also cause the loss of detailed information regarding, for instance, the coupling between the different degrees of freedom. In order to overcome this limitation and be able to gain insight on the coupling and how energy is transferred among the DOFs, we have analyzed how the character of the H_2 initial eigenstates is conserved throughout the propagation, by calculating the overlap, $\theta(z)$, between the propagated functions, Ψ, and a set of *static* H_2 eigenstates computed at several points along the nanotube axis, Φ:

$$\sigma(z,t) = \langle \Psi(\vec{R}; z, t) \mid \Phi(\vec{R}; z, t) \rangle = \\ = \int \Psi(\rho, \theta, \phi, x, y, z, t)^* \Phi(\rho, \theta, \phi, x, y, z, t) d\rho d\theta d\phi dx dy \tag{7}$$

where $\vec{R}$ stands for the degrees of freedom taken into account for the overlap. The Φ eigenstates are obtained following the same procedure described in Section 3.2 only the value of z_0 in the trapping potential is changed. The overlap between the propagated wave packet and these reference functions tells us about the distortions of the wave packets when they travel along the nanotube: if a one-to-one correspondence between the wave packets and the

bound states was found, that would mean that there are no distortions of the eigenstates due to the propagation along the nanotube, and therefore that the coupling of the z DOF with the remaining 5 is negligible. Oppositely, a large coupling would lead to a strong mixing of states during the propagation. It should be mentioned that we calculate a partial overlap function, since we integrate only in the subspace complementary to the z DOF, and therefore the overlap will depend on the total value of the wave function in that point, thus allowing us to focus the analysis on the relevant areas of the propagated wave packet at each time step. This analysis is done at several points along the z coordinate to detect how the H_2 states are distorted as they evolve along the nanotube.

4. Discussion

Employing the SA-MCTDH approach and the parameters details in Sections 3.2 and 3.3 the first 11 eigenstates of the H_2@SWCNT system were converged for a z value of the trapping potential, $z = -1.36$ bohr, corresponding to the center of a nanotube unit cell. The corresponding eigenenergies relative to the ground state are listed in Table 3. The reported energy values are in complete agreement with those of previous 5D calculations shown in Refs [16, 17]. Table 3 also contains the energies of the eigenstate calculations at values of $z = 0.73$, 2.73, 4.73 and 6.74 bohr, corresponding to alternating minima and maxima. As expected, due to the small corrugation of the potential along the z coordinate, the eigenenergies calculated at several points of the nanotube present only minor differences among them in terms of energy (tenths of wave numbers between calculations at maxima and minima).

Table 3: Computed eigenenergies (cm^{-1} units) of the H_2@SWNT system with the H_2 trapped with an harmonic potential centered at different points along the z coordinate. Ground state energies given in the first row, energy increments given for the remaining of states.

State	**ΔE (cm^{-1})**				
	$z = -1.36$	$z = 0.73$	$z = 2.73$	$z = 4.73$	$z = 6.74$
0	2744	2798	2744	2798	2798
1	71	58	58	58	71
2	157	175	175	175	157
3	157	175	175	175	157
4	253	270	270	270	253
5	253	270	270	270	253
6	396	434	434	434	396
7	409	435	435	435	409
8	409	436	436	436	409
9	428	443	448	448	428
10	430	472	468	468	430

Note that the zero point energy for this eigenstates includes $\sim$ 200 cm^{-1} corresponding to the ZPE of the harmonic trapping potential added.

As detailed in Section 3.3 the resulting initial eigenstates are next prepared for the time propagation. In order to do that, first a linear impulse is given in the z DOF and second the SPF basis of the MCTDH wave function is expanded. Two sets of propagation have been carried out here, one simulating a set of confined H_2 eigenstates traveling collinearly along the nanotube axis ($\alpha = 0°$) and an average thermal translational energy of 298 K, and

second set with same energy content but an impinging angle of $\alpha = 45°$. In both cases, the MCTDH wave function was propagated during 500 fs. In the case of the $\alpha = 0°$ propagation, the calculation implied 216 h of clocktime in a 12 core processor. For the $\alpha = 45°$ propagation, the required time was 190 h.

4.1. Projection analysis

The projection of the wave packet sets on the z coordinate shows that the corrugation of the nanotube, even though it is quite small, has a deep effect on the dynamics of the system: the wave packet does not advance as it would for a free particle, even with a considerably high kinetic energy (26 meV), but has to overcome periodic potential barriers ($\sim$ 8 meV) which give a clear structure to the function. As an illustrative example, Figure 3 displays four snapshots of the z-projection of the ground state wave packet for $\alpha = 0°$ at 0, 100, 200, and 500 fs superimposed to a schematic projection of the PES is also given (dashed line). The initially localized wave packet spreads as the propagation goes on, gaining structure due to the presence of the periodic potential. The projections also show that this propagation time is enough to separate the whole the wave packet in two fractions: the one which has enough energy to overcome the potential energy barrier created by the corrugation of the nanotube, and the one which does not have the necessary energy. The fraction of the wave packet trapped in the initial potential energy well can be estimated integrating over the region of the z coordinate which delimitates this well (from -3.34 to 0.74 bohr). In the case of the collinear ground state, we find that approximately a 23% of the initial wave packet remains trapped in the initial potential energy well after 500 fs. The amount

Table 4: Percentage of the probability density of the different wave packets that remains in the initial potential energy well after 500 fs of propagation.

$\alpha = 0°$				$\alpha = 45°$			
State	% in well	State	% in well	State	% in well	State	% in well
0	23	5	26	0	36	5	41
1	20	6	32	1	32	6	37
2	27	7	28	2	43	7	36
3	27	8	28	3	43	8	40
4	26	9	33	4	42	9	35

of wave packet trapped after the propagation is related to the overall shape of the initial wave packet, since the probability distribution in the different coordinates will affect the potential felt by the whole hydrogen molecule (Table 4). This means that some wave packets, with a higher probability density in areas of the PES which are more strongly repulsive, will have to overcome higher potential barriers than others. In this respect, note for instance that the first excited state, whose wave function presents a node in the $\theta = \pi/2$ plane, is the one with less fraction remaining trapped in the well. On the other hand, for other states with a high probability density in this region the fraction of wave function remaining in the well becomes much higher.

Concerning the remaining coordinates of the system, the respective projections show a very small variation in time, which points to a low coupling between the z coordinate and the other five DOFs. This is explained by the small corrugation of the potential along the carbon nanotube: unlike

the barrier posed for the rotation along θ and the confining potential in x and y, which are large enough to generate a coupling between the degrees of freedom [17], the changes of the PES in z are not strong enough. This lack of correlation is further confirmed by studying at the population of the last occupied natural SPF in the different DOFs as a function of time: we see clearly that the changes are of the order of 10^{-3}, which is pretty much insignificant.

Increasing the impinging angle to 45° changes significantly the outcome of the propagation to what the projection on the z coordinate is concerned. This projection is shown in Figure 4 together with the projection of the PES for 4 different time instants. As expected, since there is less effective linear momentum along the z coordinate, the amount of wave packet which remains trapped is significantly higher: around 36% for the ground state, and up to 43% for some excited states. Moreover, the distortions observed in the remaining degrees of freedom are much stronger in this case than in the previous one. The initial wave packet has a linear momentum partially pointing to the nanotube wall, and explores a region of the PES with much more corrugation along the z axis. In this new landscape, the correlation between the different degrees of freedom, mainly z, x and θ , is increased. In Figure 5 we can see the projection of the ground state wave packet with impinging angle 45 in the θ dimensions at four different time instants. These projections show how the probability distribution in θ changes in time due to the coupling with z.

4.2. Overlap study

As discussed earlier, the projection of the projected wave packets in different coordinates allows for an intuitive qualitative interpretation of the propagation, but misses more detailed information about the couplings between the degrees of freedom and the energy exchange between them. This information can be obtained by comparing the projection of the wave packets at different times with a set of static eigenstates. This states are obtained using the same trapping potential as in Section 2.2, but centered at different z values.

The overlap between the propagated wave packet and this set of static eigenstates is analyzed from two different points of view. In the first place, we focus our attention on how crossing a complete unit cell of the nanotube affects the wave packets. In order to do this, the static eigenstates are computed at $z = 6.74$ bohr, which is an equivalent point to the initial position of the wave packet ($z = -1.36$ bohr) in the neighboring unit cell. On the other hand, we are also interested on how the possible changes in the wave packets are produced. To study this, we perform the same overlap calculation with static eigenstates corresponding to several points along the z coordinate. These analysis points were selected at the critical points of the unit cell, *i. e.* the potential maxima ($z = 0.74$ and 4.73 bohr) and minima ($z = 2.73$ and 6.74 bohr). Through this approach we intend to see if the mixing occurs mainly in certain points along the nanotube, or if it is a gradual change.

The changes on a wave packet after crossing a whole unit cell are shown in figures 6 and 7, where we show the overlap functions between the ground state wave packet and the most relevant elements of the set of static eigen-

states, computed at the point $z = 6.74$ bohr. Again, we take the ground state propagation as a representative case, and discuss the changes between the different impinging angles, $\alpha = 0°$ and $45°$. Note that for both figures there is a clearly dominant overlap function, corresponding to the overlap between the wave packet and the reference function most similar to the initial state (upper panels), while the overlap with other eigenstates is comparatively much smaller. This trend is maintained for all the initial states propagated, and confirms the idea of small coupling discussed in Section 4.1. However, in spite of this common trend, we find significant differences between the collinear and the $\alpha = 45°$ propagation. The first difference between the propagations carried out at different conditions is seen in the overall shape of the dominant overlap function. It is readily seen that the decrease on this function is much sharper for the $\alpha = 0°$ propagation. This is again related with the effective linear momentum along the z coordinate, which is higher for this initial configuration. Regarding the remaining overlap functions, the differences between the collinear ($\alpha = 0°$) and the deviated ($\alpha = 45°$)propagations are even more noticeable. The collinear case presents almost no mixing of states in any of the states propagated, the most significant contributions arises from states 8 and 10 but in both cases is two orders of magnitudes smaller than the ground state contribution. This is in complete agreement with the observations made on the base of the projections in different degrees of freedom. On the other hand, in the $\alpha = 45°$ case there is a higher overlap between the wave packet and several other static eigenstates. In particular the 5th excited state at approximately 200 fs reaches a value comparable to the GS overlap. This indicates a higher dynamical coupling and exchange of

energy between the different degrees of freedom. Additionally, this coupling increases in time, as it can be seen by the fact that the main overlap function decreases, while the overlap with other states remains basically constant; t the final steps of the propagation, the proportion of mixed states reaches almost a 20%. These results are again consistent with the analysis of the projections of the wave packet.

The second part of the overlap functions' analysis, carried out at several points along the z coordinate of the nanotube, is shown in Figures 8 and 9, again, for the ground state with both impinging angles. There, the two most relevant overlap functions are plotted as a function of time for several z values (0.73, 2.73, 4.73 and 6.75 bohr). Note again the difference in scale: the primary overlap function (upper panel) is much more relevant than the secondary (lower panel). For the primary overlap, the changes in the function seem to be mainly related with the different shape of the wave packet when it crosses the different analysis points. However, if we take a look to the secondary overlap, we see a trend not noticed before: although the shape of the function is similar in all the analysis points, the overlaps at the points corresponding to a maximum in the PES ($z = 0.73$ and $z = 4.73$ bohr) are significantly higher than the ones computed in the minima ($z = 2.73$ and $z = 6.74$ bohr). Therefore, it could be argued that the positive gradients in the PES increase the mixing of states, whether the negative gradients favor a partial recovery of the initial properties of the wave packet. Therefore, for longer propagation times and farther analysis points, we should see an increase in the mixing of states, since as the wave packet travels through the nanotube, the cumulative effect of maxima and minima might blur the

properties of the initial state of the propagation.

On the other hand, for the $\alpha = 45°$ propagation we see a different behavior. This can be seen in Figure 9, which shows the two most important overlap functions for the ground state propagated with impinging angle of 45°. Note that for the final instants of the propagation the primary overlap function decreases, while the overlap with the 5th excited state, although oscillating, maintains its value. This is again prove of a higher coupling and mixing of states with respect to the collinearly diffusing H_2. However, the maxima-minima pattern observed for the collinear propagation is not clear anymore, probably due to the fact that there is a strong coupling between the x and θ DOFs induced by the linear momentum added to the x dimension: since this changes the area of the PES explored by the wave packet, it may result in a different potential energy landscape in which the analysis points do not correspond to critical points anymore.

Note that our simulations correspond to a high temperature frame. In these conditions, the kinetic energy of the molecules is, as we have already seen, enough to overcome the corrugation of the nanotube quite easily (even though not completely). Quantum confinement effects are known to be more noticeable at low temperatures [15, 18, 19]. In order to confirm this fact, we have tried to mimic an experimental setup which would allow to follow the diffusion of a single hydrogen molecule in the nanotube. This setup would use laser light to trap a molecule in a certain region of space (as does our virtual trapping potential). Then, once the laser would be turned off (we remove our trap), the molecule would evolve freely and diffuse. To reproduce computationally this experiment, we carried out a calculation letting the

system evolve freely, without modifying the momentum of the individual wave packets. Therefore, the linear momentum of the initial functions is centered at 0 eV and the simulation would correspond to the free diffusion of an eigenstate. This simulation was carried out using the same basis set as for the collinear propagation with increased initial linear momentum.

The analysis of this last propagation allows some final details of the interpretation previously presented to be discussed. Figures 10 and 11 correspond to the same analysis of the overlap functions as the one made for translationally excited wave packets: Figure 10 shows the main overlap functions for the propagation of the ground state at $z = 6.74$ bohr, and Figure 11 gathers the two main overlap functions at the same four analysis points presented before. Regarding Figure 10, we see that the shape of the main overlap function differs significantly from those of Figures 6 and 7: it is much broader and starts to be relevant at larger time values. This is clearly a result of the smaller kinetic energy of the wave packet. This difference is even more noticeable when comparing the profiles of the overlap functions at different z points: whilst in the case of increased initial linear momentum the overall shape of the main overlap function seemed to decay smoothly, in Figure 11 we see that it changes significantly. This shows again that the structure that the wave packets acquire during the propagation, as shown in Section 4.1, is much more important in this case. This is still more noticeable in some excited states like the 9th. This fact makes difficult to establish a trend in the secondary overlap functions, but in general and comparing with the systems studied with different initial conditions, the coupling is significantly higher in this case than in the collinear propagation, although not as large as in the

$\alpha = 45°$ one (Fig. 10). This indicates that an increased initial linear momentum helps the wave packet to overcome the barriers with enough kinetic energy, so that the coupling is less important. On the other hand, when the wave packet has no net initial linear momentum it explores areas with less kinetic energy, which are more affected by the potential, and therefore the coupling between the DOFs is stronger.

5. Summary and conclusions

In the present work we have presented a 6D study of the hydrogen molecule confined in Single-walled Carbon Nanotubes. The system is modeled within the rigid nanotube approach, taking into account the full coupling among all of hydrogen DOFs. The use of a virtual trapping potential to compute eigenstates highly localized in the z coordinate has provided a set of 11 physically meaningful initial states for the propagation, and in full agreement with previous studies with 5D models [16, 17]. The simultaneous propagation of these states using the SA-MCTDH approach has proved both efficient and rigorous.

We have carried out three propagations with different initial conditions. In two of them we have added a linear momentum to the center of mass of the molecule to account for a translationally excited molecule, with average kinetic energy corresponding to 298 K. In one case, the initial momentum was directed along the z coordinate, in the other one, the momentum vector formed a 45° angle with the nanotube's axis. Finally, a propagation was made without shifting the momentum distribution, in order to mimic an experimental assembly of molecular hydrogen trapping by laser cooling. The

wave function projections of the three propagations reveal a probability density structured in the z dimension, whereas the distortions on the remaining DOFs are very weak in comparison. This is taken as a first indication of the conservation throughout the propagation of the nature of each initial eigenstate. The complementary analysis relying on the calculation of the partial overlap between the propagated wave packet and sets of eigenstates calculated at different points along the carbon nanotube axis, allows us to quantify the coupling between the degrees of freedom, and shows that the wave packets with increased initial momentum collinear to the nanotube's axis are the ones with the smallest coupling, whether the ones with an initial momentum directed partially towards the nanotube's walls present a much higher mixing of states, although still not extremely high. The wave packets with zero group velocity lie somewhere in between the previous cases, showing that quantum effects are stronger at lower temperatures due to the lower kinetic energy of the particles.

The low coupling, in agreement with studies on similar systems [22], suggests that a mean-field scheme could be used in this context. Its development would allow an improvement of the model by being able to find more complex and accurate potential energy surfaces and leaving the rigid nanotube approximation behind.

6. Acknowledgements

Financial support from the Spanish Ministerio de Economía y Competitividad (Ministry of Economy and Competitiveness) (CTQ2013-41307-P) and Generalitat de Catalunya (2014-SGR-25) is acknowledged. M.M.-M. further

thanks a predoctoral grant from the FPU program (FPU2013/02210) from the Spanish Ministerio de Educación, Cultura y Deporte (Ministry of Education, Culture and Sports, Spain). The authors wish to particularly thank Prof. Uwe Manthe for his advice in the design of the propagations.

[1] X. Ren, C. Chen, M. Nagatsu, X. Wang, Carbon nanotubes as adsorbents in environmental pollution management: A review, Chemical Engineering Journal 170 (2011) 395–410.

[2] U. Mueller, M. Schubert, F. Teich, H. Puetter, K. Schierle-Arndt, J. Pastré, Metalorganic frameworksprospective industrial applications, Journal of Materials Chemistry 16 (2006) 626.

[3] R. E. Morris, P. S. Wheatley, Gas storage in nanoporous materials., Angewandte Chemie (International ed. in English) 47 (2008) 4966–81.

[4] J.-R. Li, R. J. Kuppler, H.-C. Zhou, Selective gas adsorption and separation in metal-organic frameworks., Chemical Society reviews 38 (2009) 1477–504.

[5] A. C. Dillon, K. M. Jones, T. A. Bekkedahl, C. H. Kiang, D. S. Bethune, M. J. Heben, Storage of hydrogen in single-walled carbon nanotubes, Nature 386 (1997) 377–379.

[6] H.-M. Cheng, Q.-H. Yang, C. Liu, Hydrogen storage in carbon nanotubes, Carbon 39 (2001) 1447–1454.

[7] T. Yildirim, A. Harris, Quantum dynamics of a hydrogen molecule confined in a cylindrical potential, Physical Review B 67 (2003) 245413.

[8] D. Henwood, J. D. Carey, Ab initio investigation of molecular hydrogen physisorption on graphene and carbon nanotubes, Physical Review B 75 (2007) 245413.

[9] J. L. Belof, A. C. Stern, B. Space, A predictive model of hydrogen sorption for metalorganic materials, The Journal of Physical Chemistry C 113 (2009) 9316–9320.

[10] G. E. Ioannatos, X. E. Verykios, H2 storage on single- and multi-walled carbon nanotubes, International Journal of Hydrogen Energy 35 (2010) 622–628.

[11] I. Matanovi, J. L. Belof, B. Space, K. Sillar, J. Sauer, J. Eckert, Z. Bači, Hydrogen adsorbed in a metal organic framework-5: coupled translation-rotation eigenstates from quantum five-dimensional calculations., The Journal of Chemical Physics 137 (2012) 014701.

[12] J. J. M. Beenakker, V. D. Borman, S. Y. Krylov, Molecular transport in the nanometer regime, Physical Review Letters 72 (1994) 514–517.

[13] S. FitzGerald, T. Yildirim, L. Santodonato, D. Neumann, J. Copley, J. Rush, F. Trouw, Quantum dynamics of interstitial h2 in solid c60, Physical Review B 60 (1999) 6439–6451.

[14] T. Yildirim, A. Harris, Rotational and vibrational dynamics of interstitial molecular hydrogen, Physical Review B 66 (2002) 214301.

[15] T. Lu, E. Goldfield, S. Gray, Quantum states of hydrogen and its isotopes confined in single-walled carbon nanotubes: dependence on inter-

action potential and extreme two-dimensional confinement., The journal of physical chemistry. B 110 (2006) 1742–51.

[16] J. Suarez, F. Huarte-Larranaga, Hydrogen confined in single-wall carbon nanotubes: Anisotropy effects on ro-vibrational quantum levels, The Journal of Chemical Physics 137 (2012) 064320.

[17] M. Mondelo-Martell, F. Huarte-Larrañaga, 5d quantum dynamics of the h2@swnt system: Quantitative study of the rotational-translational coupling, The Journal of Chemical Physics 142 (2015) 084304.

[18] C. I. Contescu, H. Zhang, R. J. Olsen, E. Mamontov, J. R. Morris, N. C. Gallego, Isotope effect on adsorbed quantum phases: Diffusion of h_{2} and d_{2} in nanoporous carbon, Physical Review Letters 110 (2013) 236102.

[19] Q. Wang, S. Challa, D. Sholl, J. Johnson, Quantum sieving in carbon nanotubes and zeolites, Physical Review Letters 82 (1999) 956–959.

[20] G. Garberoglio, Quantum sieving in organic frameworks, Chemical Physics Letters 467 (2009) 270–275.

[21] T. K. Nielsen, U. Bösenberg, R. Gosalawit, M. Dornheim, Y. Cerenius, F. Besenbacher, T. R. Jensen, A reversible nanoconfined chemical reaction., ACS nano 4 (2010) 3903–8.

[22] D. Skouteris, A. Laganà, Mctdh calculations on the rigid oh radical moving along a (10,0) carbon nanotube, Chemical Physics Letters 575 (2013) 18–22.

[23] R. Dovesi, R. Orlando, B. Civalleri, C. Roetti, V. R. Saunders, C. M. Zicovich-Wilson, Crystal: a computational tool for the ab initio study of the electronic properties of crystals, Zeitschrift für Kristallographie 220 (2005) 571–573.

[24] R. Dovesi, R. Orlando, B. Civalleri, C. Roetti, V. R. Saunders, C. M. Zicovich-Wilson, F. Pascale, K. Doll, N. M. Harrison, I. J. Bush, P. DArco, M. Llunell, Crystal 09 user's manual, 2009.

[25] P. Morse, Diatomic molecules according to the wave mechanics. ii. vibrational levels, Physical Review 34 (1929) 57–64.

[26] H.-D. Meyer, U. Manthe, L. Cederbaum, The multi-configurational time-dependent hartree approach, Chemical Physics Letters 165 (1990) 73–78.

[27] M. Beck, A. Jäckle, G. A. Worth, H.-D. Meyer, The multiconfiguration time-dependent hartree (mctdh) method: a highly efficient algorithm for propagating wavepackets, Physics Reports 324 (2000) 1–105.

[28] U. Manthe, The state averaged multiconfigurational time-dependent hartree approach: vibrational state and reaction rate calculations., The Journal of Chemical Physics 128 (2008) 064108.

[29] T. Hammer, U. Manthe, Iterative diagonalization in the state-averaged multi-configurational time-dependent hartree approach: excited state tunneling splittings in malonaldehyde., The Journal of Chemical Physics 136 (2012) 054105.

[30] G. Schiffel, U. Manthe, On direct product based discrete variable representations for angular coordinates and the treatment of singular terms in the kinetic energy operator, Chemical Physics 374 (2010) 118–125.

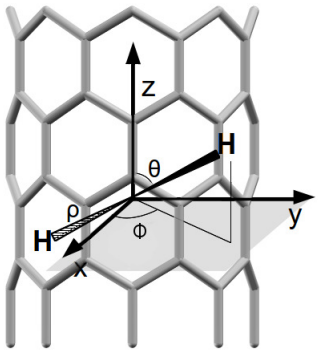

Figure 1: Scheme of the DOFs considered in the present work

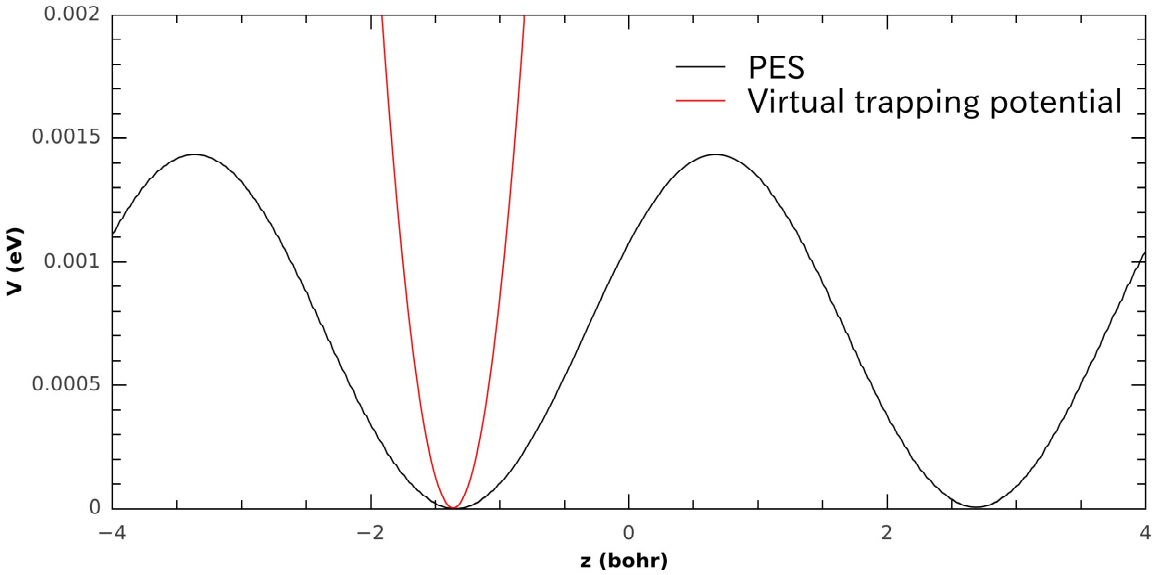

Figure 2: Representation of the projection of the PES in the z dimension (black) and the virtual trapping potential (red).

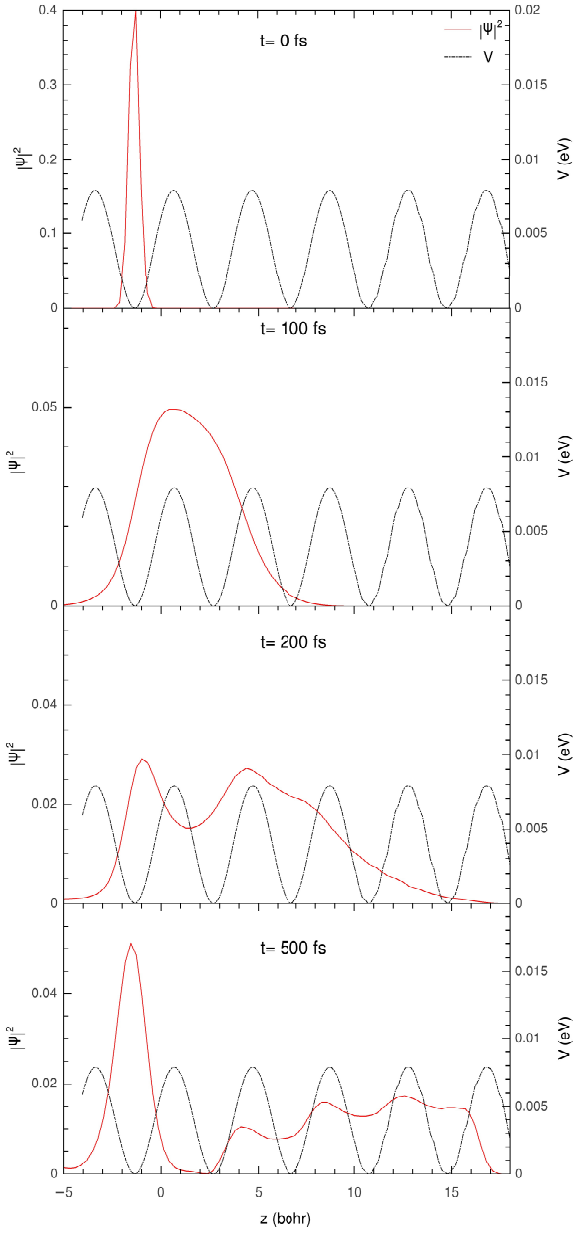

Figure 3: Several snapshots of the propagation using the bound ground state as the initial state, projected on the z coordinate. The wave packet gains structure as time advances. Note the change of scale on the axis corresponding to the probability density.

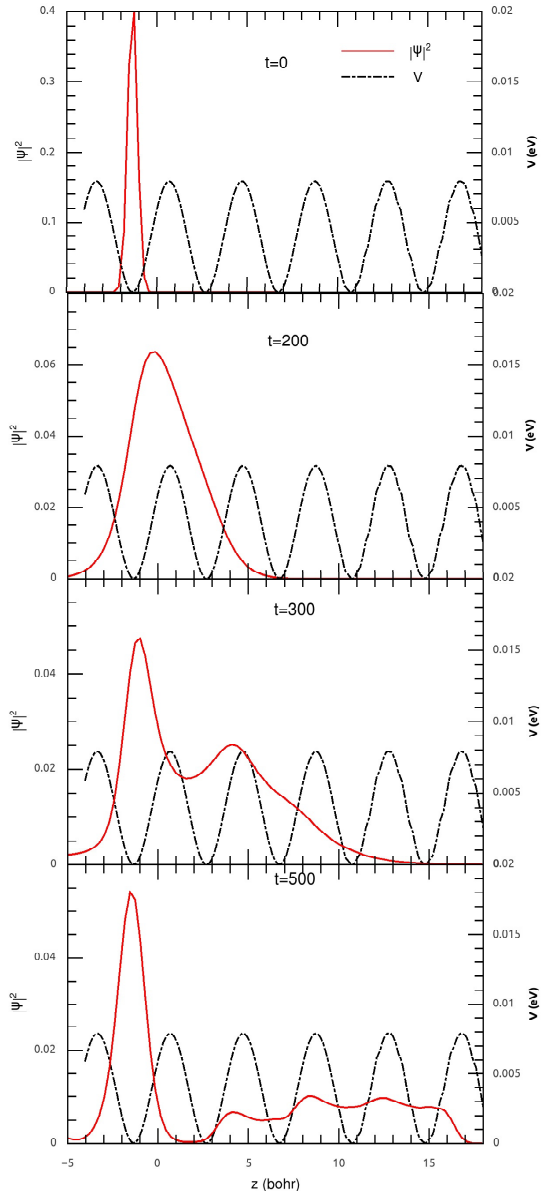

Figure 4: Snapshots of the projection of the ground state wave packet for t=0, 100, 200 and 500 fs on the z subspace.

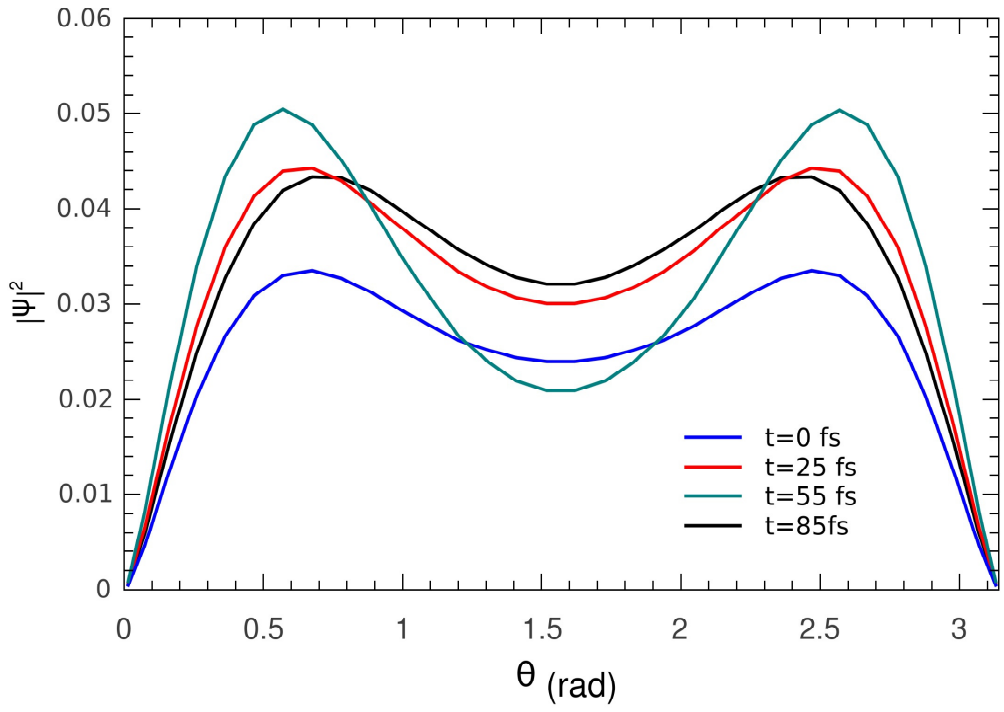

Figure 5: Projection on the θ subspace for the ground state wave packet at t=0, 25, 55 and 85 fs.

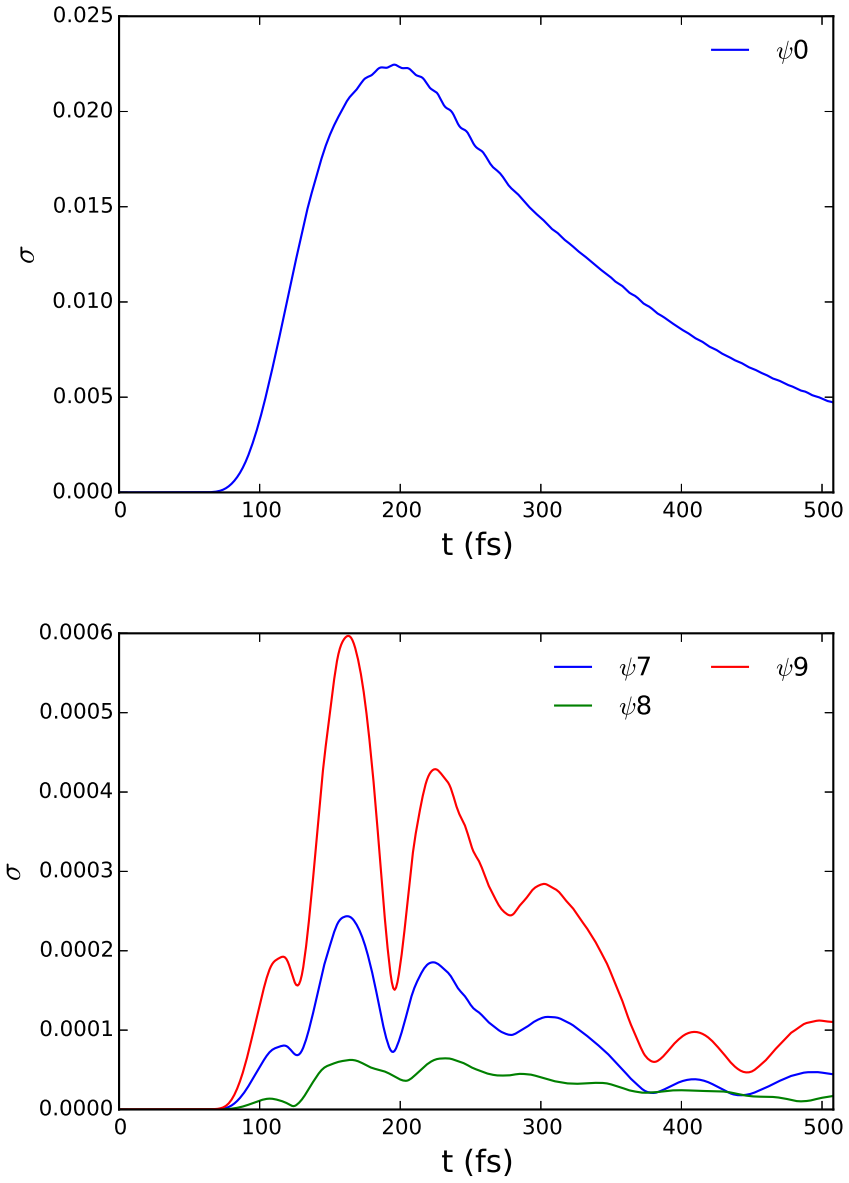

Figure 6: Value of the overlap function of the lowest energy wave packet, with $\alpha = 0°$, with 10 reference functions at $z = 6.74$ bohr. Upper panel: main overlap function, corresponding to the ground bound state. Lower panel: overlaps for the remaining relevant overlap functions

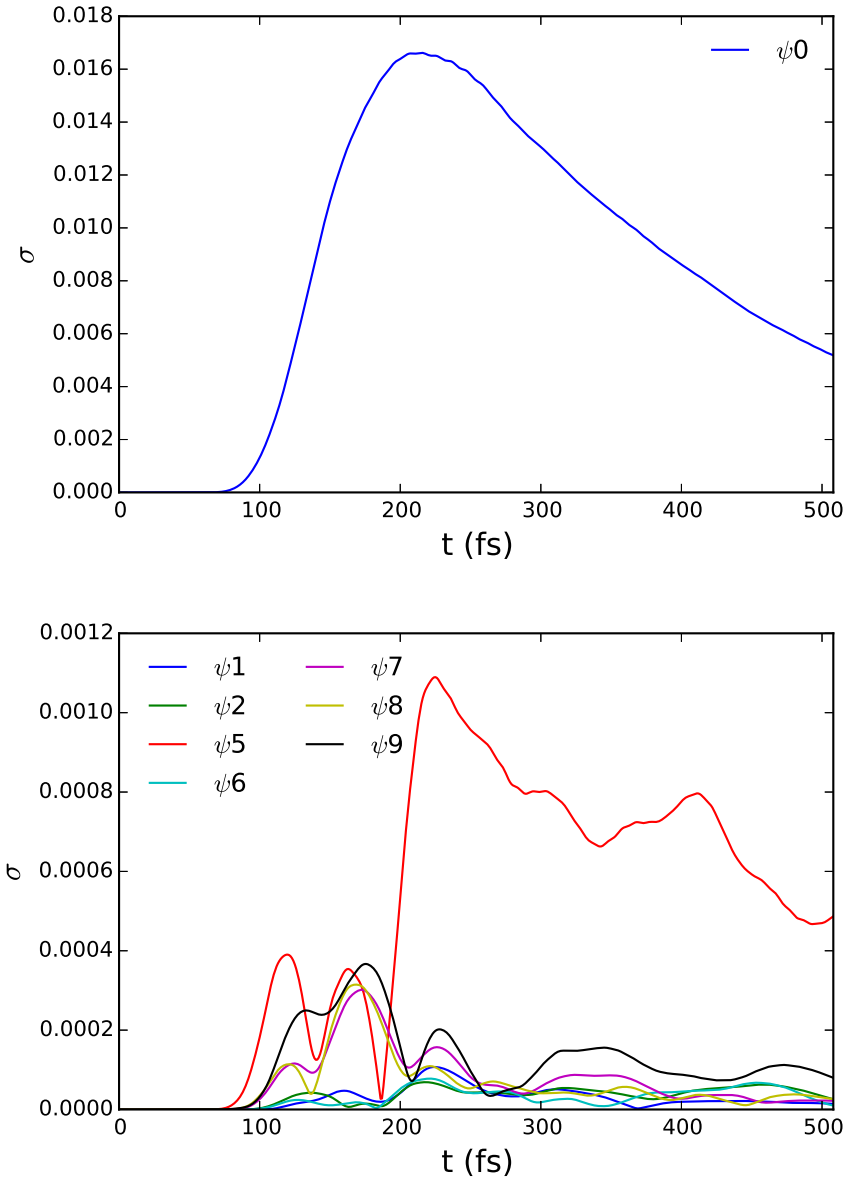

Figure 7: Value of the overlap function of the lowest energy wave packet, with $\alpha = 45°$, with 10 reference functions at $z = 6.74$ bohr. Upper panel: main overlap function, corresponding to the ground bound state. Lower panel: overlaps of the remaining relevant overlap functions.

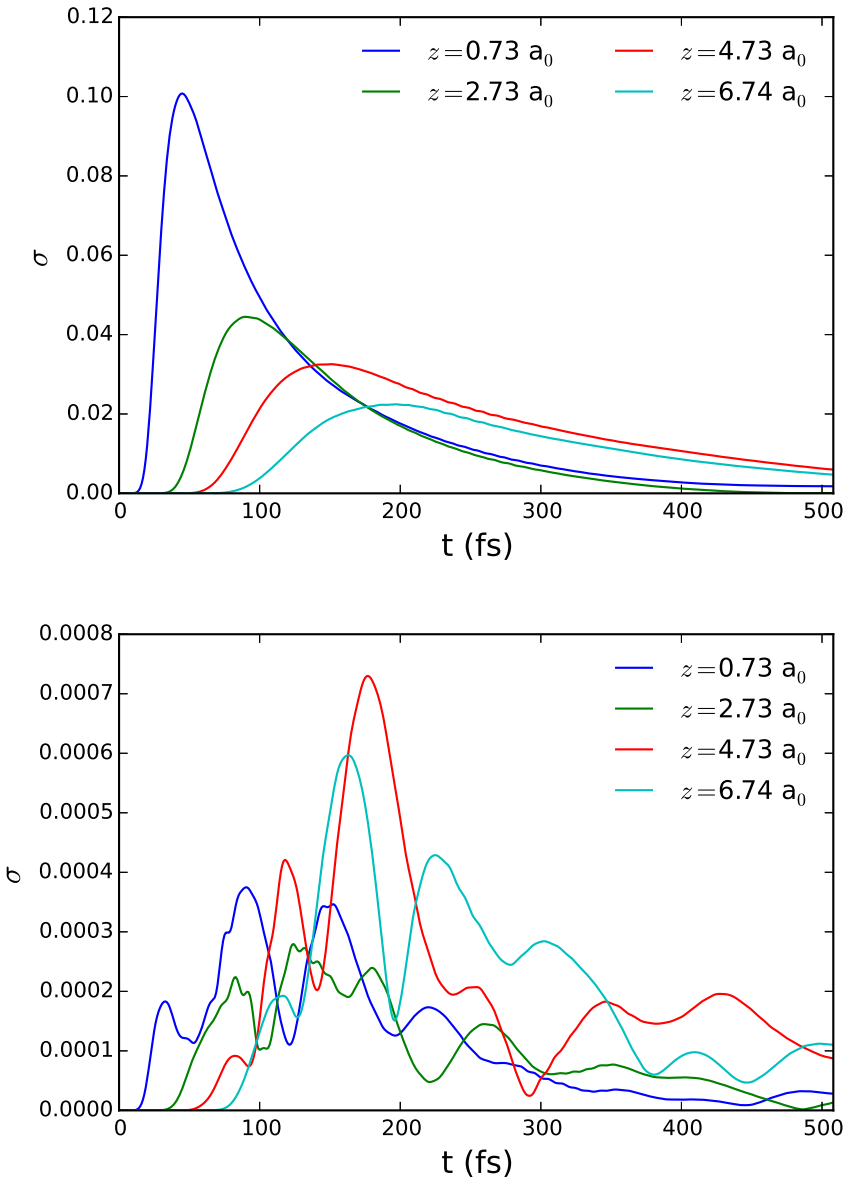

Figure 8: Value of the overlap function of the lowest energy wave packet, with $\alpha = 0°$, at 4 different points along the z coordinate. Upper panel: most relevant overlap function –see figure 6–. Lower panel: second most important overlap function.

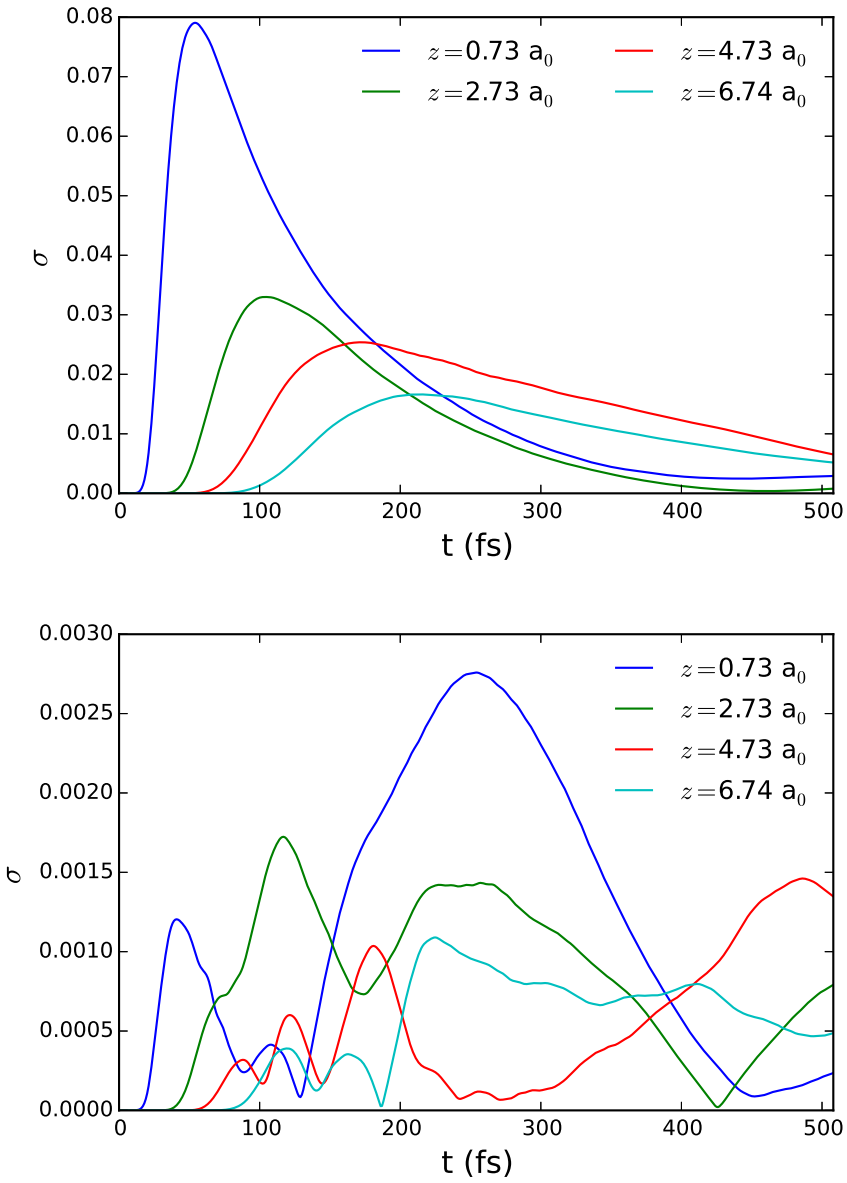

Figure 9: Value of the overlap function of the lowest energy wave packet, with $\alpha = 45°$, at 4 different points along the z coordinate. Upper panel: most relevant overlap function –see figure 7–. Lower panel: second most important overlap function.

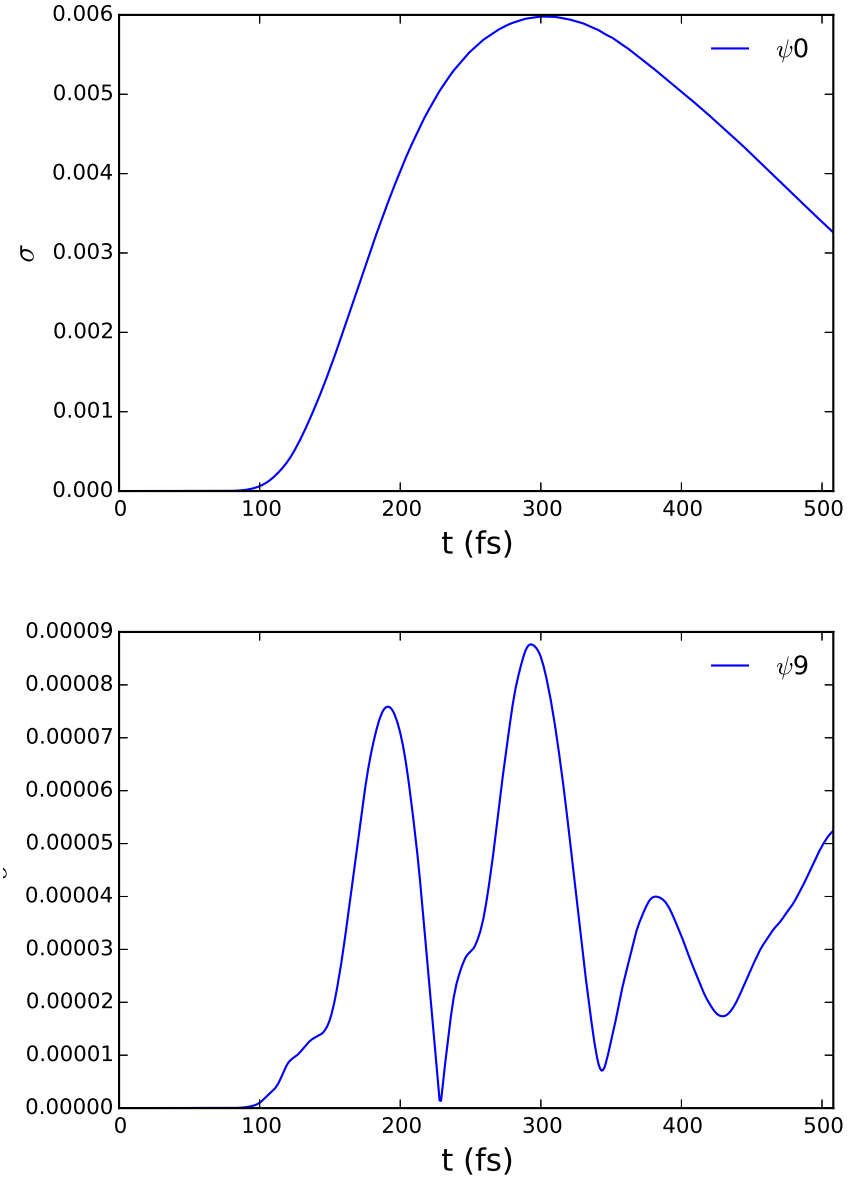

Figure 10: Value of the overlap function of the lowest energy wave packet with 0 group velocity. Upper panel: primary overlap function, corresponding to the ground bound state. Lower panel: relevant secondary overlap function corresponding the the 9th excited state. Note the difference in the maximum of probability with respect to previous states with increased initial linear momentum.

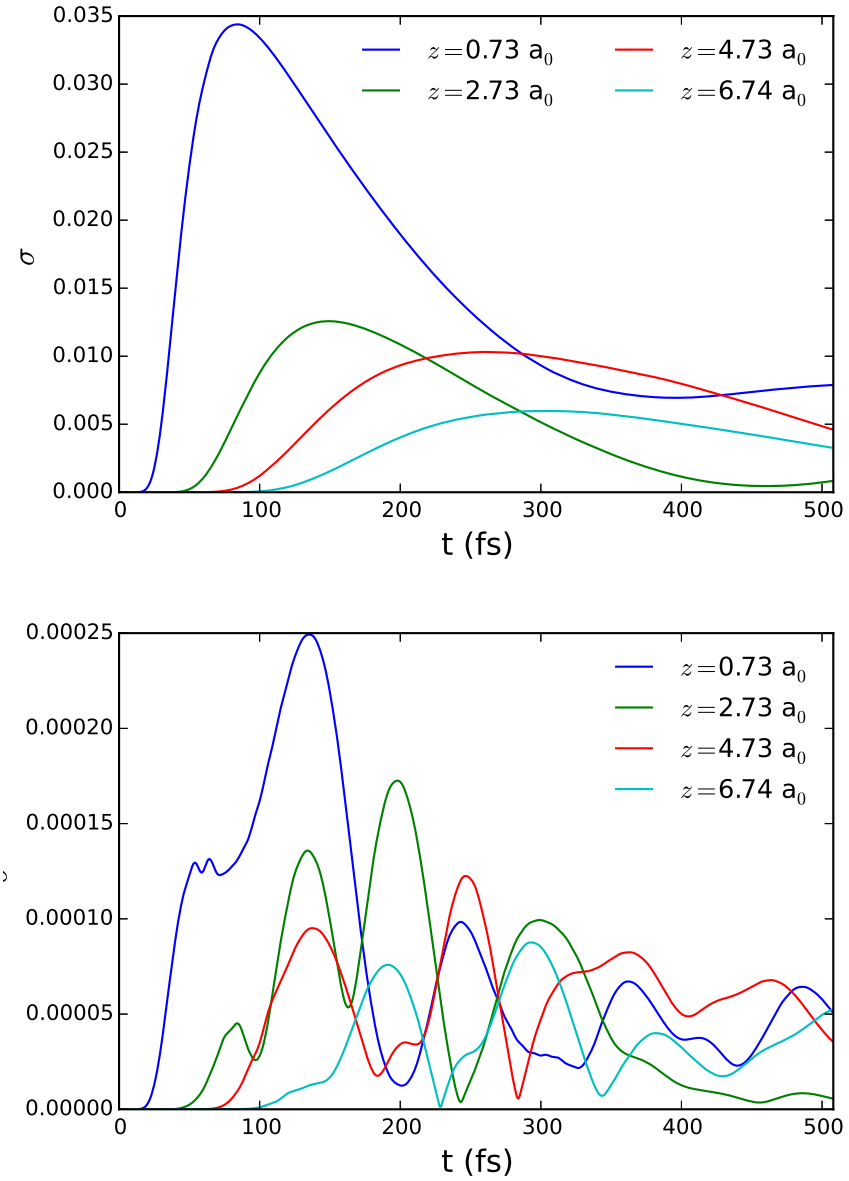

Figure 11: Value of the overlap function of the lowest energy wave packet, with $\alpha = 45°$, at 4 different points along the z coordinate.